Macromolecular Research

Article

DOI 10.1007/s13233-020-8096-y

www.springer.com/13233 pISSN 1598-5032 eISSN 2092-7673

Performance Enhancement of PVDF/$LiClO_4$ Based Nanocomposite Solid Polymer Electrolytes *via* Incorporation of $Li_{0.5}La_{0.5}TiO_3$ Nano Filler for All-Solid-State Batteries

Pazhaniswamy Sivaraj[1,2]
Karuthedath Parameswaran Abhilash[3]
Balakrishnan Nalini[4]
Pandurangam Perumal[1]
Kalimuthu Somasundaram[1,2]
Paneerselvam Christopher Selvin*[1]

[1] Luminescence and Solid State Ionics Laboratory, Department of Physics, Bharathiar University, Coimbatore-641046, India
[2] Materials Research Centre, Department of Physics, N.G.M.College, Pollachi, Coimbatore-642001, India
[3] Herbert Gleiter Institute of Nanoscience, Nanjing University of Science and Technology, Nanjing-210094, P. R. China
[4] Department of Physics, Avinashilingam Institute for Home Science and Higher Education for Women, Coimbatore -641 043, India

Received December 5, 2019 / Revised February 19, 2020 / Accepted February 22, 2020

Abstract: Experimental and computational techniques have been applied to investigate the influence of $Li_{0.5}La_{0.5}TiO_3$ nanoparticles on the ionic conductivity of the poly(vinylidene fluoride) (PVDF)/$LiClO_4$ nanocomposite solid polymer electrolyte. The theoretical evidence facilitated to suggest a plausible mechanism for Li-ion conduction across the PVDF/$LiClO_4$/$Li_{0.5}La_{0.5}TiO_3$ based solid polymer electrolytes. The solid composite polymer electrolyte with 30 wt% of $Li_{0.5}La_{0.5}TiO_3$ (LLTO) nanofiller exhibited an unprecedented ionic conductivity of 2.3687×10^{-3} S cm^{-1} at room temperature. The addition of LLTO nanoparticles to the polymer matrix enhanced its ionic conductivity by two orders of magnitude. The activation energy (E_a) and total transference number (t) were estimated to be 0.29 eV and 0.853, respectively. The interaction between the filler and polymer matrix has been inferred by the density functional theory (DFT)-IR analysis. The DFT calculations have been performed on the above system using the basis set of B3LYP-LANL2DZ. The calculated IR spectra were compared with the experimental FTIR data, which allowed us to propose accurate vibrational assignments and to clarify the complex IR vibration of the samples. All-solid-state Li_2FeSiO_4/C|PVDF/$LiClO_4$/LLTO| graphite lithium cell has been fabricated using the highest Li-ion conducting PVDF/$LiClO_4$/LLTO composite polymer electrolyte. The all-solid-state cell exhibits an excellent initial specific capacity of 87.13 and 73.24 mAh g^{-1} after 30 cycles, demonstrating higher capacity retention. The findings provide an avenue for exploring the simple all-solid-state lithium batteries, which are potential candidates for next-generation energy storage technology.

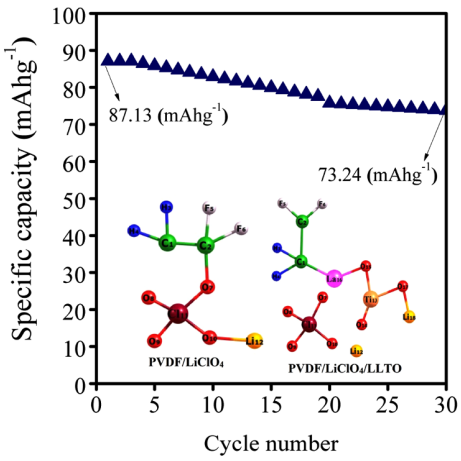

Keywords: solid polymer electrolyte, nanocomposite, DFT calculations, ionic conductivity, all-solid-state battery.

1. Introduction

In recent decades, the solid-state Lithium Polymer Batteries (LPBs) have been intensively interested in consumer electronics for low power applications, electric and hybrid vehicles due to their promising features such as low self-discharge, lightweight, no leakage, excellent compatibility *etc*.[1,2] Numerous approaches have been devoted to preparing the novel electrolytes with several polymers, such as polyacrylonitrile (PAN), poly(ethylene oxide) (PEO), poly(methyl methacrylate) (PMMA) and poly(vinylidene fluoride) (PVDF).[1-5] Among these, the PVDF becomes a favourable choice as the polymer host for gel and dry polymer electrolytes due to its promising properties such as excellent electrochemical stability, affinity to the electrolyte solution, high dielectric constant (ε = 8.4) and active electron-withdrawing functional group (-C-F-).[4] However, membrane preparation of the PVDF based polymer electrolytes becomes more difficult, and dendrite formation at electrode/electrolyte interface occurs, preventing wide utility of this in commercial lithium-ion batteries. The crystalline nature of PVDF hinders the transportation of Li^+ ions and hence batteries with PVDF based electrolytes have poor electrochemical performances.

Recent studies reveal that the composite solid polymer electrolytes alone can offer lithium polymer batteries with better electrode/electrolyte compatibilities.[6,7] One of the most promising ways to enhance the electrochemical properties of polymer electrolytes is the dispersing of ceramic nanofillers.[8] The inorganic nanoparticles hinder the polymer crystallization and a create highly conductive interface layer between the polymer matrix and filler.[9,10] The ceramic fillers for polymer matrix are

Acknowledgments: Mr. P. Sivaraj thanks to the Council of Scientific Industrial Research (CSIR), Govt. of India, New Delhi, for providing the necessary financial support through the Senior Research Fellowship (SRF) (File No:09/0472(181)-2018-EMR-I) for the present work.

***Corresponding Author:** P. Christopher Selvin (csphysics@buc.edu.in)

 © The Polymer Society of Korea and Springer 2020

two types, namely, active and passive. The active fillers like Li_2N, $LiAl_2O_3$, $Li_{1.3}Al_{0.3}Ti_{1.7}(PO_4)_3$, *etc*., participate in lithium migration process.[11] The inactive fillers, such as Al_2O_3, MgO, TiO_2, SiO_2, *etc*., are not involved in the lithium transport process.[12,13]

The ceramic nanofillers have a large surface area and effectively enhance the ionic conductivity drastically. The perovskite oxides of ABO_3 types, such as lithium lanthanum titanate ($Li_{0.5}La_{0.5}TiO_3$ (LLTO)) ceramic particles, exhibit higher solid-state Li^+ ion conductivity reported to date ~10^{-3} S cm^{-1} at room temperature.[14] The LLTO has been served as suitable ion-conducting solid-state electrolytes for all solid-state/thin-film batteries.[15] The inherent problem with this material is to prepare as thin-film electrolytes.[16] Recently very few researchers tried to prepare LLTO incorporated composite polymer films. Wei Liu *et al*.[17] reported the PAN-$LiClO_4$ composite electrolyte with the addition of 15 wt% $Li_{0.33}La_{0.557}TiO_3$ nanowire exhibits a highest ionic conductivity of 2.4×10^{-4} S cm^{-1} at room temperature. Similarly, Chunsheng *et al*.[18] have prepared PEO-$LiN(SO_2CF_2CF_3)_2$ nanocomposite system with the incorporation of $Li_{0.55}La_{0.35}TiO_3$ fiber and reported the highest ionic conductivity of 5.0×10^{-4} S cm^{-1} at room temperature when the filler content about 20 wt%. Even though several research groups have studied the PVDF-based polymer electrolytes, no special attention has been given to the preparation and characterization of PVDF/$LiClO_4$/LLTO nanocomposite polymer electrolyte.

In this work, a strategy has been made to synthesize a best composite solid polymer electrolyte by comprising of the excellent ionic conducting properties of LLTO and better mechanically stable film form capability of the PVDF/$LiClO_4$ polymer system, for the first time. The main target of the work is to explore the effect of LLTO nanoparticles on the electrical properties of PVDF/$LiClO_4$/LLTO nanocomposite polymer electrolytes. The interaction between the LLTO and PVDF/$LiClO_4$ polymer systems has been explained with the support of computational calculations. Based on the literature available so far, to the best of one's knowledge, no attempt has been made on DFT calculations for such composite polymer electrolytes. The present study also includes performing a DFT computation calculation for the composite polymer electrolytes and has been compared with the experimental results. In addition to that, an attempt has been made to fabricate all solid-state Li_2FeSiO_4/C|PVDF/$LiClO_4$/LLTO|graphite lithium polymer battery using the highest Li-ion conducting composite polymer electrolyte and the electrochemical performance of the cell has been explored by Cyclic Voltammetry (CV) analysis.

2. Experimental

2.1. Fabrication of PVDF/$LiClO_4$/LLTO nanocomposite solid polymer films

The LLTO nanoparticles were prepared by the sol-gel method.[15] The PVDF/$LiClO_4$/LLTO nanocomposite polymer electrolyte samples were prepared by the simple solution-casting method. The PVDF (Aldrich, $M_w = 6 \times 10^4$), $LiClO_4$ (AR-99.5%, Aldrich) and the LLTO nanopowders were used as raw materials. The PVDF, $LiClO_4$, and LLTO were kept in an incubator oven for 12, 12, and 5 h at 100, 120, and 120 °C, respectively. All these materials were dried separately to remove the traces of water. The *N*,*N*-dimethylformamide (DMF) was used as a solvent for preparing the composite polymer electrolytes.

For the PVDF/$LiClO_4$ preparation, the 85 wt% of PVDF polymer host was added into a beaker containing 20 mL dimethylformamide (DMF) and stirred well by using a magnetic stirrer at room temperature for 2 h. Then 15 wt% of $LiClO_4$ salt was added to the solution and stirred well for 6 h until the homogeneous viscous solution was formed. The resultant solution was poured into a Petri dish, and the residue solvent is left to evaporate at 90 °C for 12 h in an incubator oven. Similarly, the PVDF/$LiClO_4$/LLTO composite polymer electrolytes were prepared with the addition of LLTO nanoparticles. The 80 wt% of PVDF powder was first added to a beaker containing 30 mL DMF solvent and stirred well by using magnetic stirrer at room temperature for 2 h. Then 15 wt% of $LiClO_4$ salt was added to the solution and mixed by continuous stirring. Then 5 wt% of LLTO nanofiller was added to the above solution and stirred well for 6 h. The resulting homogeneous solution was poured into a Petri dish and dried at 90 °C for 12 h in an incubator oven to remove all traces of the solvent. The same procedure was applied to prepare the composite polymer electrolytes with different compositions of the LLTO filler (5, 10, 20, 30, and 40 wt%).

2.2. Characterizations

The X-ray diffraction pattern of the prepared polymer films was recorded by the Shimadzu-XRD-6000 X-ray diffractometer instrument in the range of 10-90° using monochromatic CuKα (1.5406 Å) radiation. The morphology of the samples was analyzed by Bruker-D8 AXS FE-SEM instrument. The Fourier transform infrared (FTIR) spectra were obtained by a computer interfaced Shimadzu-FTIR 220-93270-55 IR Tracer-100 spectrometer in the frequency range 500-4500 cm^{-1}. The ionic conductivity was measured using the Complex Impedance Analyzer (Hioki LCR 3532-50; Frequency range: 42 Hz to 5 MHz), where the polymer films were sandwiched between two silver electrodes. The Z-View software package processed the impedance data and it fitted with an equivalent circuit model. The transference numbers measurement was carried out by Wagner's dc polarization techniques.

2.3. All solid-state battery assembly and electrochemical characterization

The electrochemical performance of the all solid-state cell was characterized by CV and Galvanostatic charge and discharge test using two electrodes system. The all solid-state polymer battery consists of anode (graphite), cathode (Li_2FeSiO_4/C), and polymer electrolyte (PVDF/$LiClO_4$/LLTO film). The graphite was used as anode material for battery fabrication. The high capacity Li_2FeSiO_4/C nanopowder was chosen as a cathode material which was prepared by our previous report.[19] The cathode contains Li_2FeSiO_4/C and conductive carbon (Super P carbon) in the ratio of 8:2 ratio. The conductive carbon powder and Li_2FeSiO_4/C materials were mixed by mortar and pestle in order to

© The Polymer Society of Korea and Springer 2020

obtain a fine powder. In the preparation of cathode, the conductive carbon (Sigma Aldrich) was added to enhance the electronic conductivity. The anode and cathode powders were made as 1.2 mm thickness pellets and subsequently sintered at 300 °C in a tubular furnace under the Ar atmosphere. The Swagelok cell type all solid-state battery was assembled using the highest Li-ion conducting PVDF/$LiClO_4$/LLTO composite solid polymer electrolyte, which was sandwiched between the prepared anode and cathode pellets and tighten the cell. The electrochemical performance of the all solid-state Li_2FeSiO_4/C|PVDF/$LiClO_4$/LLTO|graphite lithium cell was examined by CV analysis using electrochemical system (Biologic, SP 150) with two electrodes set up. The electrochemical reversibility of the all solid-state cell was investigated for various scan rates ranging from 10 to 100 mV/s at an appropriate potential window between -2 to 2 V. The galvanostatic charge and discharge test were performed to evaluate the specific capacity of the all solid-state battery at 0.1C rate over 30 cycles.

2.4. Computational details

The structures of the $C_2H_2F_2LiClO_4$ (PVDF/$LiClO_4$) and $C_2H_2F_2$-$Li_2LaTiClO_7$ (PVDF/$LiClO_4$/LLTO) clusters were optimized by ab Initio density functional theory (DFT) calculations in order to obtain IR spectra.[20,21] The DFT computations were treated according to Becke's three parameters gradient-corrected exchange potential and the Lee-Yang-Parr gradient-corrected correlation potential B3LYP.[22] All the calculations were performed without any symmetry constraints by the Los Alamos National Laboratory 2-double-ζ LANL2DZ basis set. The single-point energy calculations were performed to study the electronic structure of the polymer complex systems using the hybrid B3LYP level of the theory[23] with the same basis set. Due to the presence of titanium (Ti) and lanthanum (La) elements, the effective core potential (ECP) was used, which effectively decreases the calculation time, and very little loss of accuracy was incurred.[24] The Los Alamos National Laboratory 2-double-ζ(LANL2DZ) basis set is popular for such metals complex system, which incorporates an ECP.[25] The DFT method employed was B3LYP/LANL2DZ, which given IR spectra of high quality and with a frequency scaling factor of 0.999, hence no scaling was applied. Artificial broadening was applied to the computed vibrational spectra only for visual interpretation of the samples. The Guassian09 quantum chemistry package performs all the calculations.[22]

3. Results and discussion

3.1. Structural analysis

Powder X-ray diffraction techniques structurally characterize the prepared PVDF/$LiClO_4$/LLTO nanocomposite polymer electrolytes. Figure 1(a) shows the typical XRD pattern of the polymer electrolyte (without LLTO filler) in which the high-intensity broad diffraction peak observed at $2\theta = 20.5°$ is ascribed to the semi-crystalline α phase PVDF and a smaller broad peak noticed at 39° is attributed to the PVDF β-phase.[26] The two characteristic reflections at $2\theta = 20.5°$ and 39° correspond to the (020) and (131)

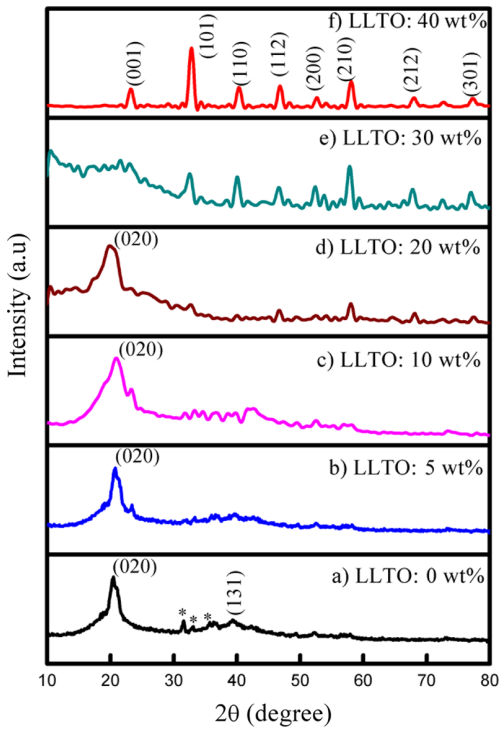

Figure 1. The XRD pattern of PVDF/$LiClO_4$/LLTO composite polymer electrolyte with the addition of different wt% of the LLTO filler.

crystallographic planes of α and β-phase in PVDF. The small intensity peaks observed at $2\theta = 31.5°$, 35.48°, and 42.15° are indexed by (111), (302), and (221) crystallographic planes of the $LiClO_4$ crystalline phase (JCPDS card no-49-0438), which are indicated by (*) in Figure 1(a).

Figure 1(b)-(f) presents the XRD pattern of nanocomposite samples. The diffraction pattern of nanocomposite electrolyte with the addition of 5 wt% LLTO filler shown in Figure 1(b). It should be noted that the peaks due to the crystalline phase of $LiClO_4$ are suppressed when the addition of LLTO nanoparticles into the host polymer. The crystalline peak (020) due to the semi-crystalline nature of PVDF is found to broaden and suppressed when compared to the filler-free sample, shown in Figure 1(c) and (d). After the addition of LLTO ceramic nanofiller, the diffraction peak of PVDF appears suppressed due to the higher concentration of LLTO ceramic filler that contributes to the higher reflectivity (Figure 1(e)).

Interestingly, the semi-crystallinity of the polymer host has vanished in the PVDF/$LiClO_4$ sample with the addition of 30 wt% of LLTO nanoparticles, which demonstrates that the LLTO nanoparticles greatly enriched the inorganic amorphous nature of the sample. However, the sample with a higher concentration (40 wt%) of the of LLTO) nanoparticles possessed some crystalline diffraction peaks which are attributed to the presence of the crystalline phase of inorganic LLTO nanofiller. The observed peaks are indexed as (001), (101), (110), (112), (200), (210), (212), and (310) crystallographic planes corresponding to a perovskite structure with the tetragonal P4/mmm space group of $Li_{0.5}La_{0.5}TiO_3$. All the peaks of $Li_{0.5}La_{0.5}TiO_3$ match well with the literature[27] (JCPDS card no:053-0109) and lattice parameters are $a = 3.871$ Å and $c = 7.737$ Å. It is noticed that the char-

 © The Polymer Society of Korea and Springer 2020

acteristic peaks of $LiClO_4$ appear completely suppressed at higher filler concentration due to the predominant concentration of LLTO over perchlorate salt. The results suggest that the incorporation of 30 wt% of LLTO nanoparticles is the optimal concentration for the polymer host to enrich the inorganic amorphous of the host polymer.

3.2. Computational study

The DFT calculations have been applied to trace the changes in the chemical bonding upon the addition of LLTO and to identify their spectroscopic manifestation. Two different clusters are developed, one $C_2H_2LiClO_4$ cluster which represents the PVDF/$LiClO_4$ complex, and one $C_2H_2Li_2LaTiClO_7$ cluster which represents the PVDF/$LiClO_4$/LLTO composite system. The interaction between the polymer matrix and filler has been carried out using the modeled clusters. The superscript on the left top of the atoms represents the numbering of atoms and subscript on the right bottom represents the number of atoms in the cluster. Figure 2(a) shows the optimized structure of the $C_2H_2F_2LiClO_4$ cluster with minimum energy obtained for structure optimizations is -916 a.u. The Lithium salt ($LiClO_4$) is incorporated into the polymer matrix, the carbon $_2$C bonded to oxygen $_7$O in the tetrahedral chlorine (ClO_4^-). The result reveals that the bridging oxygen atom ($_{11}$Cl-$_7$O-$_2$C) between the polymer matrix and Lithium salt form a whole polymer/salt complex. The calculated bond length of the $_{12}$Li-$_{10}$O bond is 1.989 Å, which is higher than all other bonds. This difference in $_{12}$Li-$_{10}$O bond should result due to the poor coordination of Lithium in the cluster.

Figure 2(b) shows the optimized structure of $C_2H_2F_2Li_2LaTiClO_7$ or ($C_2H_2F_2LiClO_4LiLaTiO_3$) cluster with minimum energy obtained for structure optimization is -976 a.u. The incorporation of the $LiLaTiO_3$ into the polymer salt ($C_2H_2F_2LiClO_4$) cluster can facilitate the ionization of the $LiClO_4$ into Li^+ cation and tetrahedron ClO_4^- anion. The ionization potential observed from DFT calculation is -60 a.u. The destruction of the tetrahedron ClO_4^- unit and Li-ion is due to the main effect of the LLTO filler. When $LiLaTiO_3$ added to the polymer salt cluster, the $_{11}$Cl-$_7$O-$_2$C (Figure 2(a)) bond is removed, and the ClO_4^- unit is separated away from carbon $_2$C, while the $_{16}$La bonded to $_1$C. The intermolecular distance between the dissociated ClO_4^- unit and the $LiLaTiO_3$ molecule is minimal (0.6087 Å), which entangles due to the strong Van der Waals interaction between ClO_4^- and $LiLaTiO_3$ but does not involve in chemical binding. The bridging of lanthanum atom between ($_1$C-$_{16}$La-$_{15}$O) LLTO and $C_2H_2F_2LiClO_4$ and structural rearrangement can lead to the formation of the perfect $C_2H_2F_2Li_2LaTiClO_7$ composite cluster.

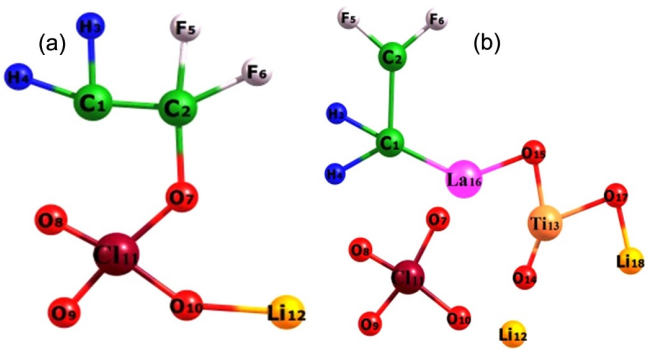

Figure 2. (a) Optimized structure of the $C_2H_2F_2LiClO_4$ cluster calculated at the B3LYP/LANL2DZ level. (b) Optimized structure of the $C_2H_2F_2Li_2LaTiClO_7$ cluster calculated at the B3LYP/LANL2DZ level: green: C, blue: H, white: F, red: O, yellow: Li, brown: Cl, pink: La, and orange: Ti.

In the LLTO, the Titanium ($_{13}$Ti) atom shared three oxygen ($_{15,17,14}$O) to form a tetrahedral TiO_3 unit and one $_{18}$Li atom bonded to oxygen ($_{17}$O) in order to maintain structural stability. The bond length of $_{16}$La-$_1$C is significantly longer than all other bonds, shown in Figure 2(b). It should be noted that an affinity would arise between nanofiller and the polymer matrix. This result suggests that the incorporation of LLTO filler reduces the coordination bonding between Li^+ and ClO_4^- in the composite polymer matrix, thereby enhances Li-ion mobility and reduces the binding energy of Li-ions which would be more favourable for the electrolyte application.

3.3. Vibrational spectral analysis

3.3.1. Theoretical and experimental IR analysis

In the present work, the theoretical IR vibrational spectra for the samples have been obtained by DFT calculations and compared with experimental spectra. Figure 3 shows the experimental and theoretical vibrational spectra of the sample without filler. Assignments are made using theoretical vibrational spectra to the experimental spectra. Figure 3(i)(a) shows the experimental FT-IR spectra of the PVDF/$LiClO_4$ sample. The characteristic peak observed at 539 cm^{-1} is attributed to the CH_2 rocking vibration of the PVDF polymer matrix. The rocking modes[28] of CF_2 vibration of β-phase is obtained at 839 cm^{-1}. The band observed at 1090 cm^{-1} is attributed to the asymmetric stretching vibration of C-C backbone of PVDF polymer. The vibrational bands at 1179 and 1230 cm^{-1} are assigned to asymmetric stretching of CF_2 and symmetric stretching mode of C-C.[26] The CH_2 wagging mode[29] is observed at 1402 cm^{-1}. The bands at 1617 and 1629 cm^{-1} are attributed to the ClO_4^- asymmetric stretching vibration and 3557 cm^{-1} due to the O-H stretching vibration.[30]

The IR spectra for the sample are calculated by DFT computational method, which allows to propose accurate vibrational assignments and to clarify the complex IR vibration of the samples. Figure 3(i)(b) shows the theoretical IR vibrational spectra of the $C_2H_2F_2LiClO_4$ cluster. The main feature of the IR spectra is indeed reproduced satisfactorily, while some minor deviations in frequency or absorbance intensity could be due to the small cluster size employed.

All the vibrational bands observed in the experimental spectra are noticed in the theoretical IR spectra with the minor deviation of frequency and absorbance intensity (5 to 10 cm^{-1} in frequency differences). The characteristics absorption band of O-H stretching vibration obtained due to absorbed water in the experiment, which is not observed in the DFT calculations because the calculations have been performed in gas phases. All the IR vibrational bands of the sample computed by DFT/ calculations are in good agreement with the experimental IR vibrational modes, which confirms the formation of perfect ($C_2H_2F_2LiClO_4$) PVDF/$LiClO_4$ complex phase.

© The Polymer Society of Korea and Springer 2020

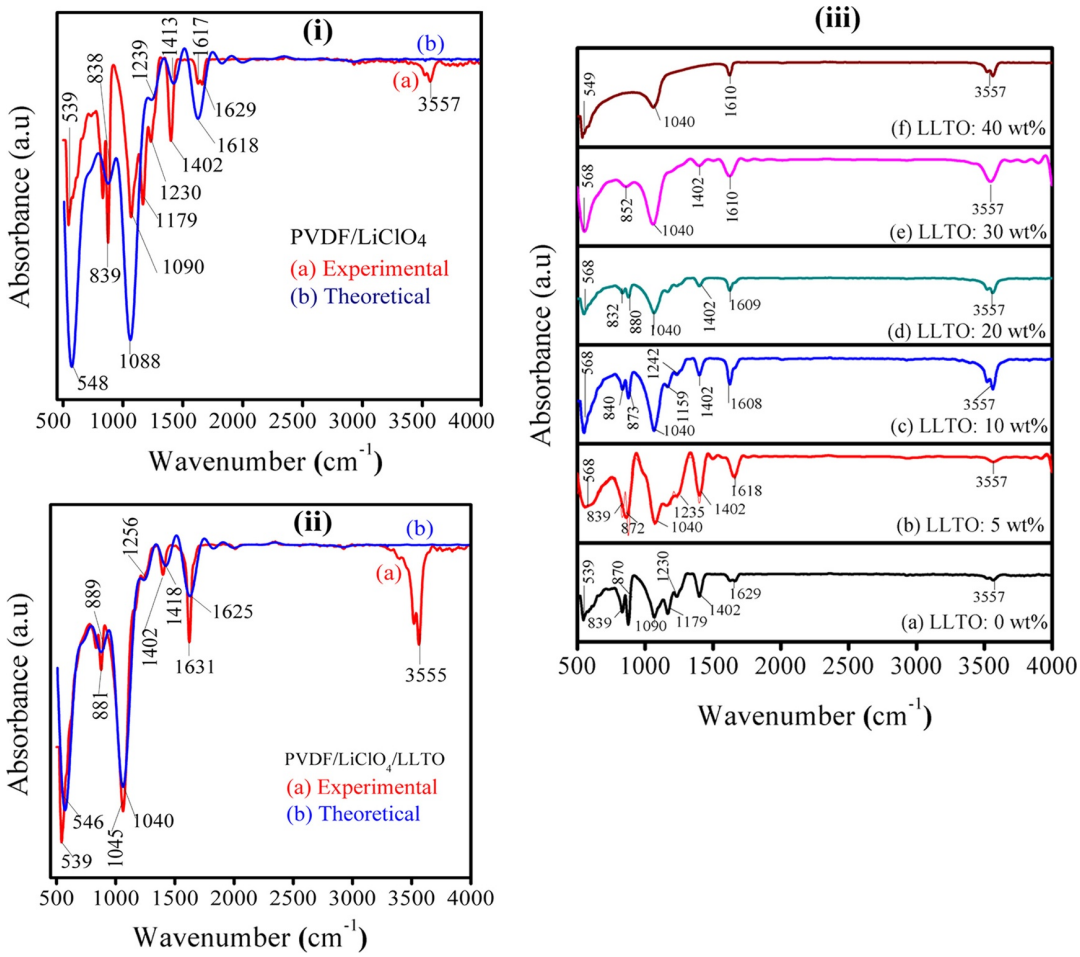

Figure 3. (i,ii) Theoretical and experimental IR spectra of PVDF/$LiClO_4$ and PVDF/$LiClO_4$/LLTO, and (iii) FTIR spectra of PVDF/$LiClO_4$/LLTO with the addition of different concentration (wt%) of LLTO filler.

Figure 3(ii) shows the experimental and theoretical IR spectra of the PVDF/ $LiClO_4$ complex with the LLTO nanofiller. Figure 3(ii)(a) shows the experimental FT-IR spectra of the PVDF/ $LiClO_4$/LLTO composite system. The vibrational bands of CH_2, CF_2, ClO_4^-, and O-H vibrations for LLTO nanofiller doped polymer electrolytes appeared in the experimental spectra are almost identical to the filler-free polymer salt complex. The sharp characteristic peak originated at 1040 cm^{-1} can be assigned to the bending vibrations of Ti-O-La bond.[16,31] The disappearance of 1090 cm^{-1} and the emergence of 1040 cm^{-1} are corresponding to the breaking of C-C bond and generation of Ti-O-La bond. The result reveals that the perfect coordination bonding of the PVDF/$LiClO_4$ and LLTO is confirmed with the addition of LLTO nanofillers into the polymer host matrix. Figure 3(ii)(b) shows the calculated IR spectra of the $C_2H_2F_2Li_2LaTiClO_7$ composite cluster. The incoporation of the LLTO filler network causes an intensity drop for vibrational modes related to CH_2, CF_2, ClO_4^-, O-H, and Ti-O-La bonding, which are clearly shown in the IR spectra (Figure 3). The vibrational modes observed at 1090, 1179, and 1230 cm^{-1} in the filler-free system are disappears when LLTO is added to the host matrix. The absence of these bands supports the mechanism of Lithium dissociation ($_{12}Li$) from ClO_4^-. The perfect PVDF/$LiClO_4$/LLTO nanocomposite complex formation has been confirmed by DFT-IR calculations.

In addition to this, the composition-dependent vibrational changes of the nanocomposite polymer electrolytes have also been investigated by experimental FT-IR analysis. The FT-IR spectra of PVDF/$LiClO_4$ and PVDF/$LiClO_4$/LLTO composite polymer electrolytes with different filler compositions are shown in Figure 3(iii).

The IR bands of CH_2 and CF_2 vibrations for 5 wt% of LLTO nanofiller doped polymer electrolytes are almost identical to the filler-free polymer salt complex. The peak originated at 1040 cm^{-1} can be assigned to the bending vibrations of Ti-O-La bond. The peak observed at 539 cm^{-1} due to CH_2 rocking vibration of PVDF/$LiClO_4$ complex polymer matrix has been shifted to a higher frequency. The stretching vibration of the CH_2 group becomes sharper while the rocking vibration of the CF_2 group is shifted to 852 from 839 cm^{-1} and vanishes for 40 wt% LLTO filler.

In Figure 3(iii)(e), the rocking vibration of CF_2 bond at 852 cm^{-1} is reduced. It is noted that the vibrational mode associated with the formation of Ti-O-La becomes more prominent and sharper with the increase in the filler concentration. There is no significant change in the peak position or emergence of new peaks. The addition of the filler varies the vibration structure. It structurally influences the intensity with respect to the concentration of LLTO, which does not change after 30 wt% filler. That may be an indication of the saturation of nanofiller reaction

 © The Polymer Society of Korea and Springer 2020

with PVDF. The sharp peaks due to the polymer filler complex bonds that emerged after the addition of LLTO nanoparticles demonstrate the strong interaction between the filler and the polymer host matrix, which has been inferred by DFT-IR calculations.

3.4. Morphological analysis

Figure 4 shows the FE-SEM micrographs of PVDF/$LiClO_4$/LLTO nanocomposite polymer electrolytes with different composition of the filler. Figure 4(a) shows the SEM micrograph of the filler-free PVDF/$LiClO_4$ system, in which the spherical particles spread over the surface with minor holes and pores. The densely packed spherical morphology of the polymer/salt complex is observed, and the average particle size is found to be 10 μm with smaller cavities. Figure 4(b), (c) shows the FE-SEM micrograph of PVDF/$LiClO_4$/LLTO composite polymer electrolyte system with the addition of 10 and 30 wt% LLTO nanofiller. The incorporation of the LLTO particles into the polymer matrix results in a uniform complex formation without any pores and holes. The complex formation results in a different morphology with an increase in the LLTO filler concentration.

The sample with 30 wt% of LLTO filler shows a uniform distribution of the particles without pores or cavities, which represent a perfect complex formation with the LLTO nanofillers embedded in the polymer matrix.

It implicates that an optimal concentration of particles yielding the most consistent composite matrix. The incorporation of ceramic particles into the polymer hosts significantly changes the nature of the morphology in the composite polymer electrolytes. Figure 4(d) shows the SEM micrograph of the composite polymer system with the addition of 40 wt% LLTO nanofillers. The rough, uneven, spherical morphology of the sample has been observed. Additionally, more and more aggregations of LLTO particles, with aggregation size slightly larger than nanosize, began to appear clearly on the surface and inside the pores of polymer electrolytes with LLTO content of 40 wt%. The photograph of the prepared PVDF/$LiClO_4$/LLTO nanocomposite solid polymer films is shown in Figure 4(e) and (f).

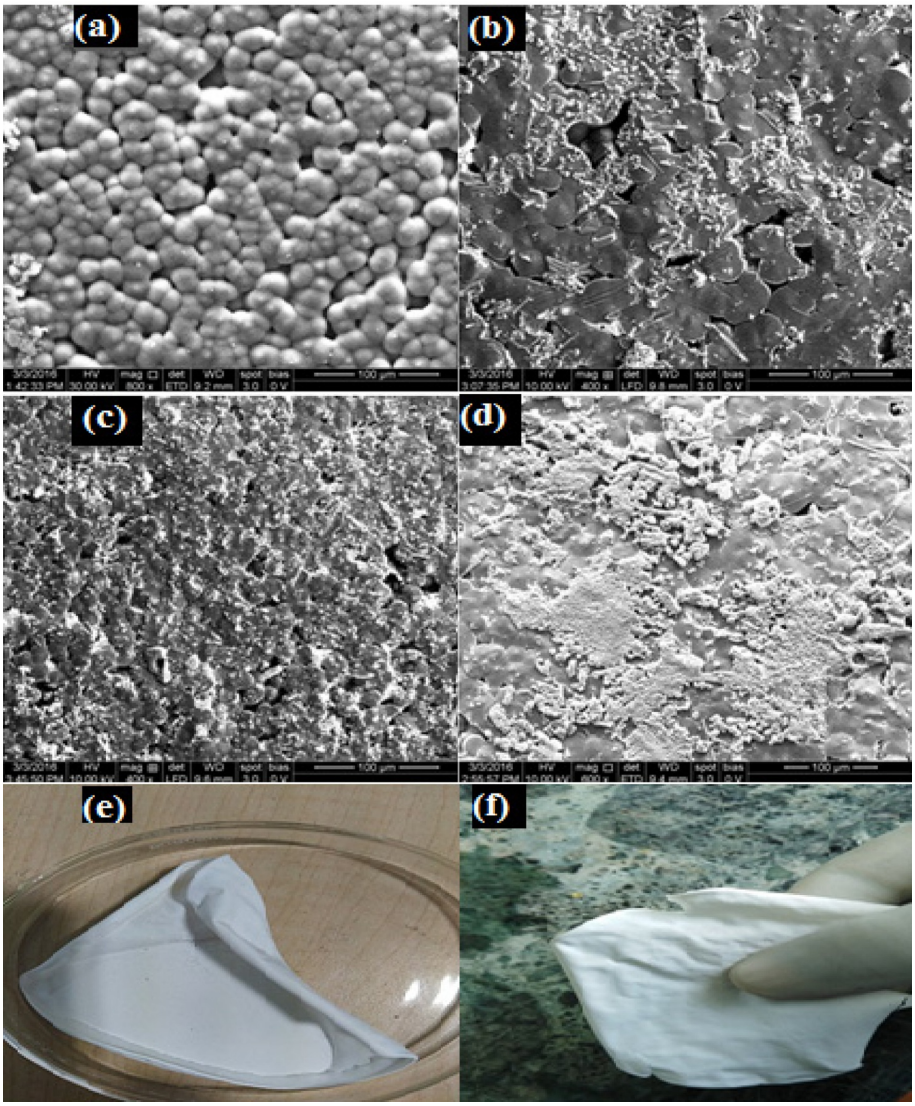

Figure 4. FE-SEM micrographs of (a) PVDF/$LiClO_4$ polymer film without LLTO filler, PVDF/$LiClO_4$/LLTO polymer films with (b) 10 wt% of LLTO filler, (c) 30 wt% of LLTO filler, and (d) 40 wt% of LLTO filler. (e,f) Photographs of the PVDF/$LiClO_4$ with 30 wt% of LLTO nanofiller.

© The Polymer Society of Korea and Springer 2020

3.5. Conductivity studies

The conductivity studies of the composite polymer samples are carried out using the complex impedance spectroscopy. Figure 5(a)-(f) shows the Cole-Cole plot (Z'(real) *vs.* Z''(imaginary) of PVDF/$LiClO_4$/LLTO composite polymer electrolytes at room temperature. The Cole-Cole plots of the sample are theoretically fitted by Z-View software, and equivalent circuits are also provided. The solid line in Figure 5 indicates the fitted plots and circles represent experimental data, and all plots show the best fitting results with the minimum error. The value of the resistance represented in the equivalent circuits. The following equation can calculate the ionic conductivity of the samples,

$$\sigma = d/A^*R_b \quad (1)$$

where the σ is the ionic conductivity, d is the thickness of the polymer films, A is the area of the composite films, and R_b is the bulk resistance of the film which can be determined from Z' *vs.* Z'' plots of the samples.

Figure 5(a) shows the Nyquist plot of the filler-free PVDF/$LiClO_4$ complex. The Nyquist plot shows a high-frequency semicircle and low-frequency semicircle with a spike, which is ascribed to the grain and grain boundary resistance of the sample. The high frequency semicircle represents the bulk relaxation of the samples; the low-frequency semicircle is due to the grain boundary effect, and straight-line after the semicircle is due to the migration of the ions[32] and the surface inhomogeneity of the contact electrodes. The total ionic conductivity of the PVDF/$LiClO_4$ film is found to be 5.680×10^{-5} S cm^{-1}. Figure 5(b) shows the Nyquist plot of PVDF/$LiClO_4$ complex with the addition of 5 wt% LLTO nanoparticles. The ionic conductivity of the 5 wt% LLTO embedded sample is found to be 1.8401×10^{-4} S cm^{-1}. In Figure 5, the high-frequency region of the Nyquist plot of filler-free and 5 wt% of LLTO incorporated PVDF/$LiClO_4$ sample slightly different from other samples due to poor grain conductivity. It has been found that the conductivity of the PVDF/$LiClO_4$ sample enhanced by the addition of LLTO nanoparticles. In Figure 5(c) and (d), the bulk resistance of the nanocomposite polymer samples decreased with the increase in the composition of the LLTO nanoparticles.

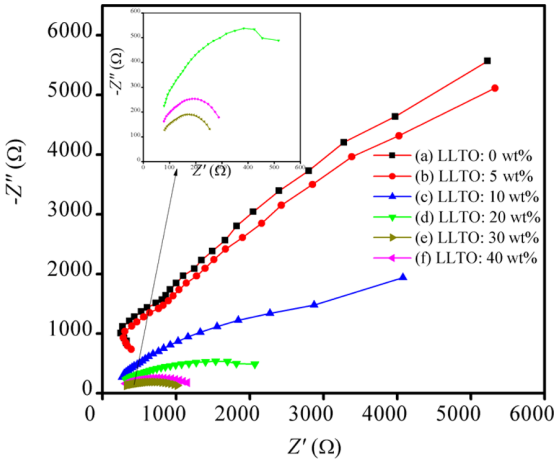

Figure 5. The Nyquist plot of nanocomposite polymer films with different concentrations of LLTO filler: (a) 0 wt%, (b) 5 wt%, (c) 10 wt%, (d) 20 wt%, (e) 30 wt%, and (f) 40 wt%.

Figure 5(e) shows the impedance spectra of the PVDF/$LiClO_4$/LLTO composite system with 30 wt% of LLTO nanofiller. An equivalent circuit has distinguished the high-frequency depressed semicircle and low-frequency semicircle of the sample. The 30 wt% of LLTO nanofiller embedded nanocomposite solid polymer system exhibits an unprecedented ionic conductivity of 2.3687×10^{-3} S cm^{-1} at room temperature (303 K), which is two orders of magnitude (10^{-5} to 10^{-3} S cm^{-1}) higher than that of the filler-free PVDF/$LiClO_4$ complex system. It is attributed to the fast ion transport on the smooth surfaces of ClO_4^- ceramic nanoparticles acting as a conductive network in the polymer complex matrix, which is further supported by morphology, XRD and DFT-IR calculations. Sethupathy *et al.*[33] reported that the SiO_2 incorporated PVDF composite nanofiber membrane exhibits the maximum ionic conductivity of 7.731×10^{-4} S cm^{-1}. Chunsheng *et al.*[18] synthesized the $Li_{0.55}La_{0.35}TiO_3$ fiber incorporated PEO-$LiN(SO_2CF_2CF_3)_2$ composite system and reported the highest ionic conductivity of 5.0×10^{-4} S cm^{-1} at room temperature when the filler content about 20 wt%. Wei Liu *et al.*[17] reported the PAN/$LiClO_4$ incorporated with 15 wt% $Li_{0.33}La_{0.557}TiO_3$ nanowire composite electrolyte exhibits an ionic conductivity of 2.4×10^{-4} S cm^{-1}.

Very recently, Mariano Romero *et al.*,[34] reported that the maximum ionic conductivity of the LLTO-PMMA composite system is 1.13×10^{-4} S cm^{-1}. In this work, the obtained highest ionic conductivity (2.3687×10^{-3} S cm^{-1}) is one order of magnitude higher than that of the previously reported by Wei Liu *et al.*, Mariano *et al.*, and Wang *et al.*[35] The obtained ionic conductivity is also higher than the bare LLTO solid-state electrolyte (1×10^{-3} S cm^{-1}).[12] The composite sample with 40 wt% of the LLTO filler drastically reduced ionic conductivity. The calculated total ionic conductivity of the nanocomposite polymer films is depicted in Table 1. From the Table 1, the conductivity of composite films increases with increase in the concentration of LLTO nanofiller up to 30 wt%. However, further addition of nanofiller higher than that of 30 wt% significantly reduces the ionic conductivity. The reduction of ionic conductivity is attributed to the ions aggregation/agglomeration of particles in the films, which has been ensured by FE-SEM analysis.

3.6. Temperature dependent ionic conductivity

Figure 6(i) shows the temperature dependence of ionic conductivity for the PVDF/$LiClO_4$/LLTO nanocomposite polymer electrolytes, the temperature ranging from 30 to 175 °C. The logσ *vs.* $1000/T$ curves for the samples appear linear, suggesting that its conductive behaviour obeys the Arrhenius equation,[36]

$$\sigma = \sigma_0 \exp(-E_a/RT), \quad (2)$$

where R is the gas constant, σ is the conductivity of polymer electrolyte, σ_0 is the pre-exponential factor, and T is temperature, respectively. It should be noted that the nanocomposite polymer electrolytes exhibit positive temperature-dependent conductance. The activation energy for Li-ion transportation has been obtained from the slope of the straight line according to the Arrhenius equation. The activation energy of filler-free

 © The Polymer Society of Korea and Springer 2020

Table 1. The ionic conductivity and activation energy of the PVDF/$LiClO_4$/LLTO composite polymer electrolytes

Samples	Total conductivity (S cm^{-1})	Activation energy (eV)
LLTO: 0 wt%	5.68×10^{-5}	0.77
LLTO: 5 wt%	1.84×10^{-4}	0.55
LLTO: 10 wt%	4.07×10^{-4}	0.44
LLTO: 20 wt%	5.54×10^{-4}	0.43
LLTO: 30 wt%	2.36×10^{-3}	0.29
LLTO: 40 wt%	7.40×10^{-4}	0.57

and LLTO embedded composite polymer electrolytes are listed in Table 1.

The 30% of LLTO incorporated PVDF/$LiClO_4$/LLTO nanocomposite solid polymer possessed very lower activation energy of 0.29 eV. The lower E_a indicates the minimum energy required for Li-ion transportation across the composite films. It suggestes that the activation energy decreases from 0.67 to 0.29 eV with an increase in the concentration of LLTO filler up to 30 wt%. The result demonstrates that the incorporation of the LLTO nanoparticles into the PVDF/$LiClO_4$ electrolytes effectively improved the lithium-ion transportation across the composite polymer electrolytes. The 40 wt% of LLTO embedded composite polymer films exhibit higher activation energy (E_a) in comparison to the 30 wt% LLTO incorporated sample, which evidence that the film exhibits lower ionic transportation across the sample. Figure 6(ii) shows the ionic conductivity and activation energy (E_a) as a function of the concentration of LLTO in the composite polymer films. It can be observed that the 30 wt% LLTO embedded PVDF/$LiClO_4$ composite system exhibits excellent ionic conductivity and low activation energy, which corresponds to low binding energy and high mobility of lithium ions.

In this work, the DFT calculations have been performed for proposing a mechanism of the ionic conductivity of the samples using the modeled ($C_2H_2F_2LiClO_4$ and $C_2H_2F_2Li_2LaTiClO_7$) clusters. This study gives, for the first time structural insights into PVDF/$LiClO_4$/LLTO nanocomposite polymer electrolytes and an attempt to a facile understanding of the observed increase in ionic conductivity by incorporating LLTO filler into the polymer matrix. Depending on the nature of filler, the following parameters have been proposed to influence the ionic conductivity of PVDF/$LiClO_4$/LLTO systems: (i) the relative amount of nanofillers, (ii) the nature of bonding in the complex, (iii) the electrostatic interaction for ion transportation, (iv) mobility and concentration of free Li^+ ion.

The LLTO incorporated into the polymer matrix, which causes sizeable structural re-origination of polymer/salt complex. When the LLTO is added to the polymer matrix, the lithium ($_{12}Li$) ion and the tetrahedral ClO_4^- unit is found to separate from the composite polymer structures (Figure 2(b)). This effect is manifested clearly by the increase of the Li-ion mobility upon the addition of LLTO filler. The intermolecular distance between the active site of ClO_4^- unit to the filler is very small, 0.6087 Å, and shown in Figure 2(b), which means that the high affinity can be expected between ClO_4^- and surface of nano-oxides. For the filler-free system, the bond length of the $_{12}Li$-$_{10}O$ is 1.9890 Å, while the bond has broken when the filler is added to the polymer matrix. In terms of filler and polymer interactions, this trend suggests a reduction of binding energy for Li-ion in the composite system. The binding energy depends strongly on the nature of the bonding in the complex network.

Along with this line, the lower electrostatic interaction between the $_{12}Li$-ions and their perchlorate sites in the composite system decreases the binding of $_{12}Li$-ions thereby improved the ionic conductivity of the sample. A real mechanism with theoretical evidence of ion transportation in the composite polymer electrolytes has not yet been reported in the literature.[9] In the present work, the DFT cluster calculations yielded an evident clue for understanding the most plausible mechanism of ionic conductivity in the PVDF/$LiClO_4$/LLTO nanocomposite solid polymer electrolytes. The theoretical evidence for the enhancement of ionic conductivity with the addition of inorganic nanofiller also has in good agreement with the Lewis acid-base theory.[37] It

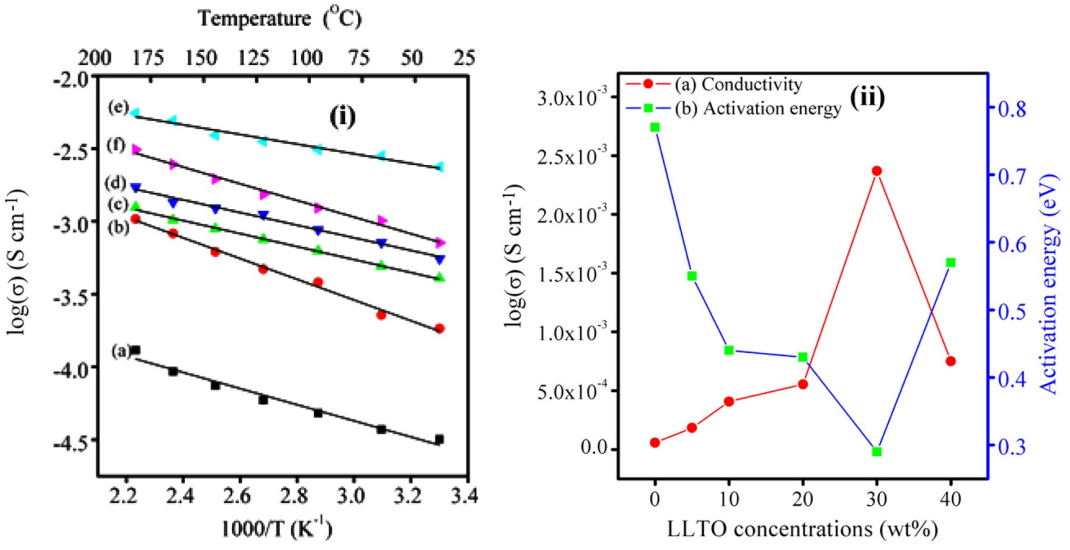

Figure 6. (i) Temperature-dependent ionic conductivity, (ii) ionic conductivity and activation energy versus different wt% of LLTO concentration of PVDF/$LiClO_4$/LLTO electrolytes.

© The Polymer Society of Korea and Springer 2020

suggests that the strong affinity can arise between the ClO_4^- and acid groups on the surface of nano-oxides, which facilitates the formation Li^+ and ClO_4^- ion pairs and results in an increase in the concentration of free Li^+.[38] These mobile Li-ions could make a random walk through the improved amorphous PVDF matrix, and the LLTO surface region is enriched with vacancies that allow Li^+ to hop from one site to the next one. However, the conductivity due to the enriched amorphous PVDF host is dominant.

3.7. Complex modulus spectroscopic analysis

Complex modulus analysis is an alternative strategy to explore the electrical properties of the composite polymer electrolytes and to magnify any other effects present in the polymer film as a result of different relaxation time constants.[39] The relation between the impedance data and electric modulus is given below

$$M^* = M' + jM'' \quad (3)$$

$$M' = \omega C_o Z' \text{ and } M'' = \omega C_o Z'' \quad (4)$$

where the M' and M'' are real and imaginary part of the complex modulus, the geometric capacitance $C_o = \varepsilon_o A/L$, A is the area of the polymer film, L is the thickness of the film and ε_o is the permittivity of the free space (8.854×10^{-14} F/cm). The variation of the real part (M') of electrical modulus with the frequency of composite solid polymer electrolytes shown in Figure 7(i). It was observed that, all the samples the M' approaches to zero for all the films, which suggest that the contribution from the electrode effect is negligible. Small dispersion is noticed in the intermediate frequency, which demonstrates the appearance of electrolyte polarizations. The M' is found to disperse at high frequency is due to the conductivity relaxation. The M' increases with an increase in the frequency for all the samples, which is attributed to the conduction phenomenon arising due to the short-range mobility of free charge carriers. The M' strongly depends on the concentration of the LLTO nanoparticles, which indicates that the space charge polarization and conductivity relaxation are depend on the contribution of LLTO nanoparticles into the polymer host matrix.

Figure 7(ii) shows the imaginary part (M'') of electrical modulus as a function of frequency for all the composite polymer films. The M'' increases with an increase in frequency and attains maximum value (peak) at a particular frequency, which shifts to a higher frequency with increases in the concentration of LLTO nanoparticles. The peak in the M'' *vs.* frequency plot is a non-Lorentzian type curve indicating the spread of relaxation time. The peak position can be attributed to the re-orientation relaxation process of mobile Li-ions.[40]

3.8. Dielectric analysis

The variation in the dielectric constant is a clear indication of polarization due to the transportation of mobile ions, electronic polarization and lattice vibrations.[41,42] The complex permittivity is given below,

$$\varepsilon_r = \varepsilon' + j\,\varepsilon'' \quad (5)$$

where the ε' is the real part of the complex permittivity or dielectric constant and ε'' is the dielectric loss during each cycle of the electric field. Figure 8(i) shows the frequency dependence of dielectric constant (ε') for different concentrations of LLTO at room temperature.

For all the samples, the frequency dispersion of dielectric constant is found to be more prominent in the low frequency. The ε' displays a frequency-independent behavior at a frequency higher than log5 (HZ). The dielectric constant ε' decreases with increases in frequency due to the electrical relaxation process. It is observed that the incorporation of LLTO nanoparticles, ε' value, is increased in the lower frequency and is constant at higher frequency regions. The LLTO incorporation causes more localization of charge carriers with mobile Li-ions which enhanced the ionic conductivity. The higher dielectric constant and strong dispersion at low frequency are due to the effects of LLTO fillers on the ionic migration in the PVDF/$LiClO_4$ complex systems. The variation of the imaginary part of dielectric permittivity (ε'') as a function of frequency for different concentrations of LLTO particles into the polymer host is shown in Figure 8(ii). The higher value at the low-frequency region is attributed to the free charge motion in the composite polymer films. The dielectric loss factor (ε'') increases with increases in the concentration of LLTO up to 30 wt% at low-frequency region which is

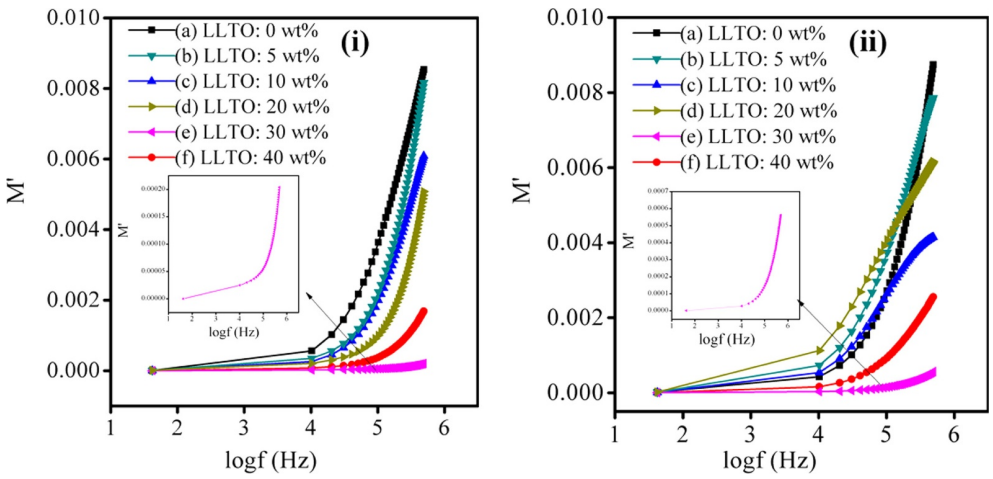

Figure 7. Electrical modulus spectra of the samples: (i) the real part (M') versus log(f) and (ii) the imaginary part (M'') versus log(f).

 © The Polymer Society of Korea and Springer 2020

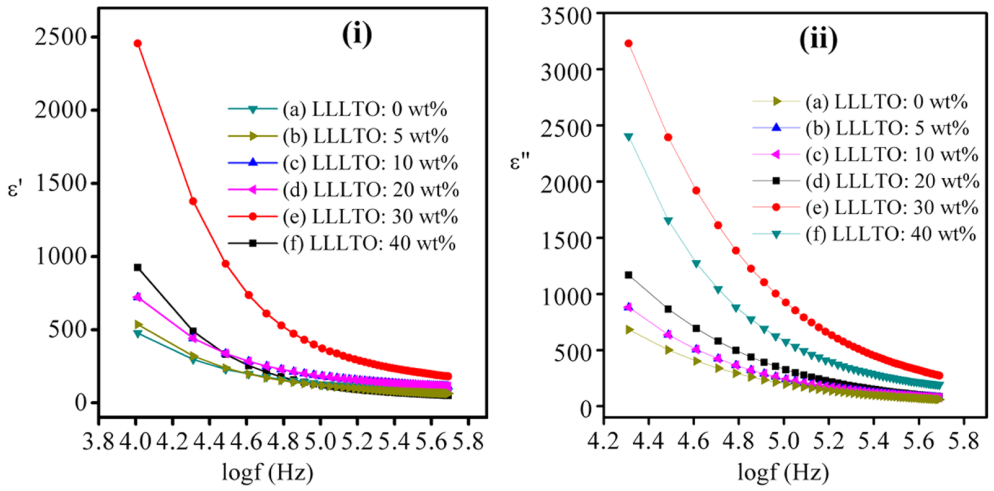

Figure 8. Dielectric spectra of the samples: (i) dielectric constant (ε') versus log(f) and (ii) dielectric loss (ε'') versus log(f).

due to the enhancement of mobility of the charge carriers. The ε'' found to decreases at higher concentration (40 wt%) might be ion aggregations. The dielectric and electrical modulus analysis for the PVDF/$LiClO_4$/LLTO based nanocomposite solid polymer has not yet been reported in the literature background.[17,34] These results facilitate to understand the mechanism for the higher ionic conductivity in the PVDF/$LiClO_4$ solid polymer electrolytes with the addition of different wt.% of LLTO filler.

3.9. Transference number measurement

The electrical conductivity measurement provides the electronic and ionic transportation mechanism in the solid polymer electrolytes. The contribution of ionic conductivity in the total conductivity of a solid polymer electrolyte plays a significant role in determining the best performance of the lithium polymer battery. The determination of the total transference number contributes to the particular charge carriers (electrons/ions) that occur in the composite polymer electrolytes. The total transference number for the PVDF/$LiClO_4$/LLTO nanocomposite solid polymer electrolytes has been elucidated by Wagner's polarization technique.[43] The ionic transference number has been obtained by the polarization current versus time plots using the equation

$$t_{ion} = (I_i\text{-}I_f)/I_i \text{ and } t_{ele} = I_f/I_i, \quad (6)$$

where the I_i is the initial current and I_f is the final current. The dc polarization measurements on the PVDF/$LiClO_4$/LLTO composite system have been carried out with silver blocking electrodes by supplying a 1.0 V DC bias voltage at room temperature.

Figure 9 shows the DC polarization current versus time plots of the PVDF/$LiClO_4$ and different wt% of LLTO filler embedded composite solid polymer electrolytes. It should be noted that all plots show the higher polarization current at the very beginning, then its value decreases instantaneously and reaches constant value after long polarization time. The larger current at the beginning is attributed to the migration of charge carriers (ions and electrons) across the polymer electrolytes. The ionic transportation number of the PVDF/$LiClO_4$/LLTO nanocomposite solid polymer electrolytes has been calculated and listed in Table 2. The total ionic transference number increases with increase in the concentration of LLTO filler and reaches a high value of 0.801 at 30 wt% of LLTO. The enhanced total ionic transference number of the composite polymer electrolytes is attributed to the enhanced density of mobile Lithium ions in the systems.

The results reveal that the charge migration in this polymer electrolyte is predominantly due to the ions with the negligible contribution of electrons. The higher transference number of the PVDF/$LiClO_4$/LLTO nanocomposite solid polymer facilitates to craft a high performance all solid-state polymer batteries.

3.10. Electrochemical performance of the all solid-state cell

In this work, the battery performance has been tested for the highest Lithium-ion conducting nanocomposite polymer electrolyte. In the case of solid-state polymer electrolyte, the ionic conductivity and transference number play an immense role in determining the battery performance of the samples. All solid-state Li_2FeSiO_4/C|PVDF/$LiClO_4$/LLTO|graphite lithium polymer battery has been constructed using the highest Li-ion conducting PVDF/$LiClO_4$/LLTO composite polymer electrolyte, for the first time. The open-circuit voltage of the constructed all solid-state lithium cell is 1.72 V (shown in Figure 10(a)), and it was stabilized, the cell has discharged connecting through 100 kΩ load resistance at room temperature. During the discharge through a load, OCV of the cell has been initially decreased, and the observed voltage of 1.62 V is monitored for 147 h.

This constant region of the cell voltage acts as a plateau region. The all solid-state battery fabrication facilitates to find the compatibility of the PVDF/$LiClO_4$/LLTO solid polymer electrolyte with the electrodes. The results suggested that the Li_2FeSiO_4/C|PVDF/$LiClO_4$/LLTO|graphite all solid-state battery possessed optimal OCV voltage and a constant plateau voltage. Further, the electrochemical performance of the all solid-state cell has been examined by CV analysis. Figure 10(b) shows the CV curve of the Li_2FeSiO_4/C|PVDF/$LiClO_4$/LLTO|graphite cell at differ-

© The Polymer Society of Korea and Springer 2020

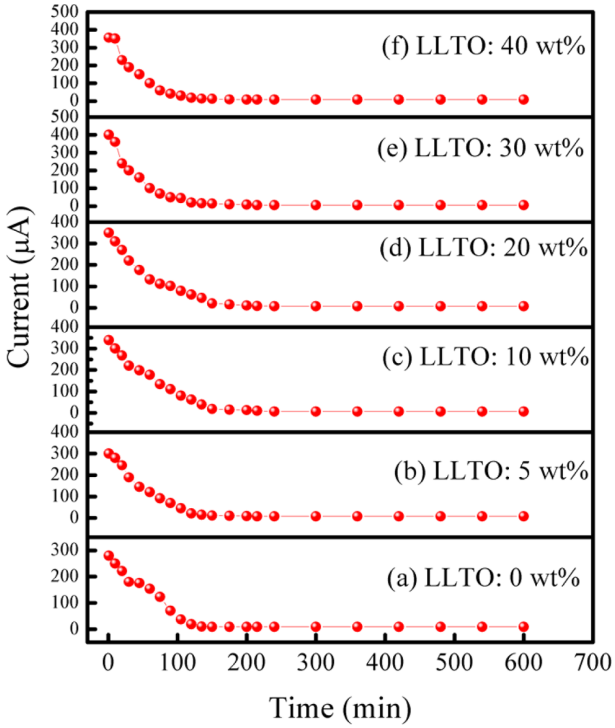

Figure 9. Current versus dc polarization time of PVDF/$LiClO_4$/LLTO composite solid polymer electrolytes.

Table 2. Total transference numbers of the PVDF/$LiClO_4$/LLTO nanocomposite solid polymer electrolytes

Samples	Transference number (t)
LLTO: 0 wt%	0.673
LLTO: 5 wt%	0.706
LLTO: 10 wt%	0.762
LLTO: 20 wt%	0.787
LLTO: 30 wt%	0.853
LLTO: 40 wt%	0.793

ent scan rates from 10 to 100 mV/s ramped between -2 to 2 V. It is noted that a pair of redox peak is observed at peak separation potential of 0.432 V. The potential difference between oxidation and reduction peaks is the key factor for evaluating the reversibility of the electrochemical reaction in the solid-state cell. The rechargeable all solid-state cell exhibits minimum peak separation potential which demonstrates the best electrochemical reversibility of the cell.

The anodic peak is attributed to the oxidation of Fe ions by the intercalation of Li-ions from Li_2FeSiO_4 /C cathode material, and cathodic peak is the reduction of Fe ions by the de-intercalation of Li-ions into the host composite. The Galvanostatic charge and discharge test have been performed for the Li_2FeSiO_4/C|PVDF/$LiClO_4$/LLTO|graphite cell at 0.1 C rate over 30 cycles shown in Figure 10(c). The all solid-state cell exhibits an excellent initial specific capacity of 87.13 and 73.24 mAh g^{-1} after 30 cycles which demonstrates the higher capacity retention. The unprecedented specific capacity of the cell is attributed to the excellent compatibility, excellent ionic conductivity and better transference number of the PVDF/$LiClO_4$/LLTO solid polymer electrolyte. The CV measurements at different scan rates have also been used to estimate the Li-ion diffusion coefficient of the all solid-state cell. The diffusion coefficient of the cell can be determined by Randles-Sevcik equation[44] which can be used to explore the effect of scan rate on peak current I_p. The linear plots of I_p *vs.* $V^{1/2}$ provide the evidence for chemically reverse redox process in the all solid-state cell shown in Figure 10(d). The diffusion coefficient of the cell is found to 1.23×10^{-11} cm^2s^{-1}. The preliminary findings provide an avenue for exploring the simple all solid-state lithium polymer batteries, which is a potential candidate for next-generation energy storage technology.

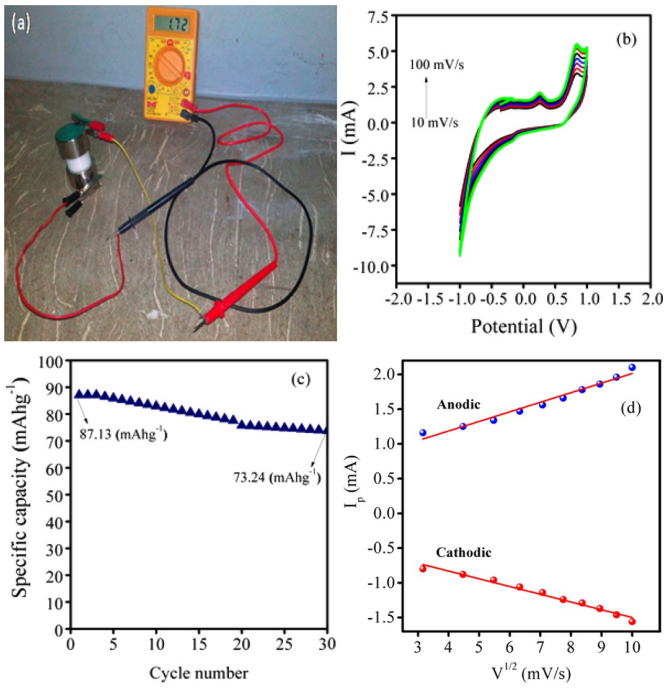

Figure 10. Rechargeable all-solid-state Li_2FeSiO_4/C|PVDF/$LiClO_4$/LLTO| graphite lithium cell: (a) photograph of the OCV measurement, (b) CV curves with different scan rate (10 to 100 mV/s), (c) specific capacity over multiple cycles, and (d) linear plot between I_p versus $V^{1/2}$ for the all-solid-state lithium battery.

4. Conclusion

The impact of the LLTO nanofiller on the ionic conductivity and electrochemical properties of the PVDF/$LiClO_4$/LLTO solid polymer has been explored. The nanocomposite polymer electrolyte with 30 wt% of LLTO exhibits an unprecedented ionic conductivity of 2.3687×10^{-3} S cm^{-1} at room temperature. The obtained highest ionic conductivity upon the addition of filler into the polymer matrix is attributed to the reduction in the binding energy of Li-ions, and it makes a random walk through the enriched amorphous host matrix. The higher transference numbers for the sample is attributed to the charge migration in the polymer electrolytes predominantly due to ions with negligible electronic conduction. The incorporation of LLTO filler in the composite polymer films has been inferred by DFT-IR calculations and compared with experimental FT-IR spectroscopic data. The theoretical spectral assignments have been made for the nanocomposite system that clarifies the complex IR vibration of this new elec-

 © The Polymer Society of Korea and Springer 2020

trolyte. The understanding of the possible mechanism on adding ceramic nanofiller, LLTO, is made clear using DFT analysis and found true by experimental analysis. The all solid-state Li_2FeSiO_4/C|PVDF/$LiClO_4$/LLTO|graphite lithium battery has been fabricated using the highest Li-ion conducting composite polymer electrolyte and electrochemical performance of the battery has been explored by CV analysis. The all solid-state cell exhibits an initial specific capacity of 87.13 mAh g^{-1} which demonstrated that the PVDF/$LiClO_4$/LLTO composite polymer electrolyte possessed excellent compatibility with the solid electrodes.

References

(1) H. S. Min, J. M. Ko, and D. W. Kim, *J. Power Sources*., **119**, 469 (2003).
(2) B. Scrosati, F. Croce, and L. Persi, *J. Electrochem. Soc*., **147**, 1718 (2000).
(3) H. S. Kim, J. H. Shin, S. I. Moon, and S. P. Kim, *Electrochim. Acta*, **48**, 1573 (2003).
(4) H. Lu, J. Du, C. Yu, X. Wang, Y. Gao, W. Xu, A. Liu, X. Lu, and Y. Chen, *Macromol. Res*., DOI: 10.1007/s13233-020-8073-5 (2020).
(5) S. C. Ryu, J. Y. Kim, C. Cho, and W. N. Kim, *Macromol. Res*., **28**, 118 (2020).
(6) G. B. Appetecchi, F. Croce, L. Persi, F. Ronci, and B. Scrosati, *J. Electrochem. Soc*., **147**, 4448 (2000).
(7) L. M. Bronstein, R. L. Karlinsey, K. Ritter, C. G. Joo, B. Stein, and J. W. Zanziger, *J. Mater. Chem*., **14**, 1812 (2004).
(8) J. W. Kim, K. S. Ji, J. P. Lee, and J. W. Park, *J. Power Sources*, **119**, 415 (2003).
(9) A. M. Stephan and K. S. Nahm, *Polymer*, **47**, 5952 (2006).
(10) X. Qian, N. Gu, Z. Cheng, X. Yang, E. Wang, and S. Dong, *Electrochim. Acta*, **46**, 1829 (2001).
(11) Y. J. Wang, Y. Pan, and D. Kim, *J. Power Sources*, **159**, 690 (2006).
(12) A. C. Balazs, T. Emrick, and T. P. Russell, *Science*, **314**, 1107 (2006).
(13) K. Malekshahinezhad, A. A. khaneghah, and H. Behniafar, *Macromol. Res*., DOI: 10.1007/s13233-020-8067-3 (2019).
(14) Inugama, C. Liquan, M. Itoh, T. Nakamura, T. Uchida, H. Ikuta, and M. Waki har, *Solid State Commun*., **86**, 689 (1993).
(15) K. P. Abhilash, P. Christopher Selvin, B. Nalini, K. Somasundaram, P. Sivaraj, and A. Chandra Bose, *J. Phys. Chem. Solids*, **91**, 114 (2016).
(16) K. P. Abhilash, P. Sivaraj, P. Christopher Selvin, B. Nalini, and K. Somasundaram, *Ceram. Int*., **41**, 13823 (2015).
(17) W. Liu, N. Liu, J. Sun, P. C. Hsu, Y. Li, H. W. Lee, and Y. Cui, *Nano Lett*., **15**, 2740 (2015).
(18) C. Wang, X. W. Zhang, and A. J. Appleby, *J. Electrochem. Soc*., **152**, 205 (2005).
(19) P. Sivaraj, B. Nalini, K. P. Abhilash, D. Lakshmi, P. Christopher Selvin, and P. Balraju, *J. Alloys Compds*., **740**, 1116 (2018).
(20) W. Kohn and L. Sham, *J. Phys. Rev*., **140**, 1133 (1965).
(21) R. G. Parr and W. Yang, *Density-Functional Theory of Atoms and Molecules*, Oxford University Press, Oxford, Clarendon, 1989.
(22) A. D. Becke, *J. Chem. Phys*., **98**, 5648 (1993).
(23) B. Miehlich, A. Savin, H. Stoll, and H. Preuss, *Chem. Phys. Lett*., **157**, 200 (1989).
(24) P. J. Hay and W. R. Wadt, *J. Chem. Phys*., **82**, 299 (1985).
(25) C. Lee, W. Yang, and R. G. Parr, *Phys. Rev B*, **37**, 785 (1988).
(26) S. S. Chio, Y. S. Lee, C. W. Joo, S. G. Lee, J. K. Park, and K. S. Han, *Electrochim. Acta*, **50**, 339 (2004).
(27) D. T. Swamy, K. E. Babu, and V. Veeraiah, *Bull. Mater. Sci*., **36**, 1115 (2013).
(28) C. L. Yang, Z. H. Li, W. J. Li, H. Y. Liu, Q. Z. Xiao, G. T. Lei, and Y. H. Ding, *J. Membr. Sci*., **495**, 341 (2015).
(29) L. O. Faria and R. L. Moreira, *J. Polym. Sci. B: Polym. Phys*., **38**, 34 (2000).
(30) X. Zhen, L. Zhang, M. Shi, L. Li, L. Cheng, Z. Jiao, W. Yang, and Y. Ding, *Macromol. Res*., **28**, 266 (2020).
(31) Y. Z. Zhang and C. K. Chan, *J. Phys. Chem. A*, **107**, 5956 (2003).
(32) P. G. Pickup, *Chem. Soc. Faraday. Trans*., **86**, 3631 (1990).
(33) M. Sethupathy, V. Sethuraman, and P. Manisankar, *Soft Nanoscience Lett*., **3**, 37 (2013).
(34) M. Romero, R. Faccio, and A. W Mombru, *Mater. Lett*., **172**, 1 (2016).
(35) L. Wang, W. Yang, X. D. Li, and G. Evans, *Electrochem. Solid State Lett*., **13**, 7 (2010).
(36) Z. X. Wang, X. J. Huang, and L. Q. Chen, *Electrochem. Solid State Lett*., **6**, 40 (2003).
(37) W. Wieczorek, Z. Florjanczyk, and J. R. Stevens, *Electrochim. Acta*, **40**, 2251 (1995).
(38) A. Dawar and A. Chandra, *Phys. Lett. A*, **376**, 3604 (2012).
(39) S. Stramare, V. Thangadurai, and W. Weppner, *Chem. Mater*., **15**, 3974 (2003).
(40) L. Simon, L. Ruban, and A. Kumar, *Mater. Res. Innov*., **21**, 249 (2017).
(41) Y. Ding, P. Zhang, Z. Long, Y. Jiang, and F. Xu, *J. Alloys Compds*., **487**, 507 (2009).
(42) X. Wu, J. Huang, S. Yu, P. Ruan, R. Sun, and C.-P. Wong, *Macromol. Res*., DOI: 10.1007/s13233-020-8049-5 (2019).
(43) S. A. Hashmi and S. Chandra, *J. Mater. Sci. Eng*., **34**, 18 (1995).
(44) P. Sivaraj, K. P. Abhilash, B. Nalini, P. Christopher Selvin, S. Goel, and S. K. Yadav, *J. Am. Ceram. Soc*., **103**, 1685 (2020).

Publisher's Note Springer Nature remains neutral with regard to jurisdictional claims in published maps and institutional affiliations.